Nanotechnology

PAPER

Excitation of hybridized Dirac plasmon polaritons and transition radiation in multi-layer graphene traversed by a fast charged particle

To cite this article: Kamran Akbari *et al* 2018 *Nanotechnology* **29** 225201

View the article online for updates and enhancements.

Related content

- Plasmonics in Dirac systems: from graphene to topological insulators
  Tobias Stauber
- Terahertz Josephson plasma waves in layered superconductors: spectrum, generation, nonlinear and quantum phenomena
  Sergey Savel'ev, V A Yampol'skii, A L Rakhmanov et al.
- Active graphene plasmonics for terahertz device applications
  Taiichi Otsuji, Vyacheslav Popov and Victor Ryzhii

This content was downloaded by silvinasegui from IP address 168.96.255.109 on 23/04/2018 at 20:02

IOP Publishing Nanotechnology
Nanotechnology 29 (2018) 225201 (13pp) https://doi.org/10.1088/1361-6528/aab53f

Excitation of hybridized Dirac plasmon polaritons and transition radiation in multi-layer graphene traversed by a fast charged particle

Kamran Akbari[1], Zoran L Mišković[1,2,6], Silvina Segui[3,4], Juana L Gervasoni[3,4,5] and Néstor R Arista[3,5]

[1] Department of Applied Mathematics, University of Waterloo, Waterloo, Ontario, N2L 3G1, Canada
[2] Waterloo Institute for Nanotechnology, University of Waterloo, Waterloo, Ontario, N2L 3G1, Canada
[3] Centro Atómico Bariloche, Comisión Nacional de Energía Atómica, Av. Bustillo 9500, 8400 S.C. de Bariloche, Argentina
[4] Consejo Nacional de Investigaciones Científicas y Técnicas of Argentina (CONICET), Argentina
[5] Instituto Balseiro, Universidad Nacional de Cuyo, Argentina

E-mail: kakbari@uwaterloo.ca, zmiskovi@uwaterloo.ca and segui@cab.cnea.gov.ar

Received 22 December 2017, revised 27 February 2018
Accepted for publication 8 March 2018
Published 29 March 2018

Abstract

We analyze the energy loss channels for a fast charged particle traversing a multi-layer graphene (MLG) structure with N layers under normal incidence. Focusing on a terahertz (THz) range of frequencies, and assuming equally doped graphene layers with a large enough separation d between them to neglect interlayer electron hopping, we use the Drude model for two-dimensional conductivity of each layer to describe hybridization of graphene's Dirac plasmon polaritons (DPPs). Performing a layer decomposition of ohmic energy losses, which include excitation of hybridized DPPs (HDPPs), we have found for $N = 3$ that the middle HDPP eigenfrequency is not excited in the middle layer due to symmetry constraint, whereas the excitation of the lowest HDPP eigenfrequency produces a Fano resonance in the graphene layer that is first traversed by the charged particle. While the angular distribution of transition radiation emitted in the far field region also shows asymmetry with respect to the traversal order by the incident charged particle at supra-THz frequencies, the integrated radiative energy loss is surprisingly independent of both d and N for $N \leqslant 5$, which is explained by a dominant role of the outer graphene layers in transition radiation. We have further found that the integrated ohmic energy loss in optically thin MLG scales as $\propto 1/N$ at sub-THz frequencies, which is explained by exposing the role of dissipative processes in graphene at low frequencies. Finally, prominent peaks are observed at supra-THz frequencies in the integrated ohmic energy loss for MLG structures that are not optically thin. The magnitude of those peaks is found to scale with N for $N \geqslant 2$, while their shape and position replicate the peak in a double-layer graphene ($N = 2$), which is explained by arguing that plasmon hybridization in such MLG structures is dominated by electromagnetic interaction between the nearest-neighbor graphene layers.

Supplementary material for this article is available online

Keywords: graphene, plasmon, energy loss, transition radiation, electron beam

(Some figures may appear in colour only in the online journal)

[6] Author to whom any correspondence should be addressed.

 © 2018 IOP Publishing Ltd Printed in the UK

1. Introduction

Both experimental and theoretical investigations of the collective electron excitation modes in doped graphene have played important roles over the past decade in the subfield of photonics research concerned with the range of frequencies from terahertz (THz) to mid-infrared (MIR) [1–3]. Namely, single layer of heavily doped graphene with large area supports a low-frequency mode known as Dirac plasmon polariton (DPP), which exhibits several technologically attractive features in that frequency range [4, 5]. Specifically, the DPP dispersion relation can be conveniently tuned via changing the chemical potential in graphene by applying potential to external gates, while the associated electric fields exhibit superior confinement perpendicular to graphene, as well as long propagation distances along graphene [6].

While the main effort of research in this area is aimed at designing optoelectronic and plasmonic devices with optimal functionalities, interactions of graphene with externally moving charged particles have also attracted substantial interest in recent years, e.g., in the context of using electron energy loss spectroscopy (EELS) to explore plasmonic properties of both single-layer graphene (SLG) and multilayer graphene (MLG) in a broad range of frequencies [7–9]. On the other hand, joining global effort to design a stable, highly tunable source of THz radiation, there have been several recent proposals to use electromagnetic radiation from graphene induced by a fast electron beam, moving either parallel [10, 11] or normal to graphene [12], where the electron velocity may be used as tuning parameter. Moreover, in order to elucidate the role of retardation effects in EELS, we have recently developed a fully relativistic treatment of the energy losses and transition radiation (TR) from doped graphene probed by a fast electron in a transmission electron microscope (TEM) [13, 14]. In that context, it may be worthwhile mentioning that the experimental setting of a TEM allows for measurements of cathodoluminescence light emission from a target [15, 16], which could be adapted to perform angle-resolved measurements of TR from graphene [17].

Over the past several years, growing effort has been invested in developing optoelectronic devices using layered structures that contain stacks of multiple layers of graphene [18–24]. Other examples of applications of MLG include radiation absorbers at sub-THz frequencies [25] and ultrasensitive THz biosensors [26, 27]. Graphene layers in such applications are usually well separated, so that so the only interaction between their electronic systems is due to electromagnetic fields. As a result, a key novel mechanism arises in the optical response of such MLG based devices due to strong hybridization among the DPP modes of individual graphene layers, which opens the possibility of using the geometric design of such structures to achieve eigenmodes with various dispersion relations and oscillator strengths in the THz to MIR frequency range.

Theoretical investigation of such MLG structures was initially concerned with plasmon hybridization in double-layer graphene (DLG), first studied by Hwang and Das Sarma [28], followed by other authors [29–31]. Plasmon hybridization in MLG systems with $N \geqslant 2$ layers was theoretically studied by Zhu *et al* [32], Stauber [33], and Rodrigo *et al* [23], among other authors. Those authors have found that, for an MLG with N layers, there exist N hybridized DPP (HDPP) modes with eigenfrequencies $\omega_j(k)$, for $j = 1, 2, \ldots N$, where k is an in-plane wavenumber. The spread among those frequencies was found to generally increase with decreasing interlayer distance(s), so that the highest-lying hybrid mode with frequency, say, ω_N merges with the light line, $\omega = ck$, at long wavelengths and approached the typical $\omega_N \propto \sqrt{k}$ dependence of a two-dimensional (2D) electron gas at shorter wavelengths [4], whereas the remaining $N - 1$ hybrid modes with lower frequencies exhibit quasi-acoustic dispersions at long wavelengths [32]. Thus, while the highest mode is always strongly affected by retardation effects at the wavelengths of interest in the THz range [34], the lower lying modes are pushed further below the light line $\omega = ck$ by decreasing interlayer distance, and are therefore less affected by retardation.

Several applications of MLG rely on the properties of the highest HDPP mode in optically thin structures, such that their thickness is much smaller than the characteristic wavelength of that mode. In that limit one may represent the conductivity of an MLG as a sum of conductivities of independent graphene layers [18, 22–24, 26, 27]. As a result, it was shown that an optically thin MLG may exhibit considerably higher effective doping density than in an SLG, which could give rise to a larger oscillator strength, as well as a higher eigenfrequency of its highest HDPP mode in comparison to the DPP mode in a SLG [23]. On the other hand, there has also been an increasing interest in the past several years to exploit dispersion relations associated with the acoustic plasmon modes in graphene for various applications [35, 36]. For example, it was recently shown that radiation sources could be developed at THz frequencies based on excitation of the low-frequency quasi-acoustic HDPP hybrid modes in an MLG by an electron beam moving parallel to graphene at a moderate speed [37, 38]. We remark that such acoustic modes can be produced, not only in an MLG structure with electronically decoupled graphene sheets [28, 32, 33], as discussed above, but also in an SLG in the presence of a nearby metal gate [35], or in a structure that combines those two designs, namely, an MLG on a conducing substrate [36].

With all the above mentioned intricacies regarding the dispersion relations and oscillator strengths of the HDPP modes in MLG structures, and in view of a diverse range of their applications, we find it timely to expose some new features of MLG at THz frequencies when such structures are traversed by a fast external charged particle. Since we are interested in the limit of extremely long wavelengths associated with those frequencies, we adopt the Drude model, which was shown to describe rather well the DPP mode in a doped graphene by means of an in-plane optical conductivity [5, 39]. Specifically, in this work we analyze the effects of the number of layers N and the interlayer distance on the energy

loss of a fast charged particle traversing the MLG, as well as the resulting TR from those layers in the THz range of frequencies. We only consider a somewhat idealized system represented by a stack of graphene layers suspended in free space in order to emphasize the role of plasmon hybridization between graphene layers by eliminating screening, or possible additional hybridization with collective modes due to the presence of a substrate or dielectric spacer layers [40]. By choosing such a system we also focus on TR from graphene layers, while eliminating Cherenkov radiation in a substrate [41], as well as TR arising when the charged particle traverses a dielectric boundary.

While fully relativistic formulation of the N-layer problem was presented in our previous paper, results were discussed for the case of a DLG only [14]. Specifically, we have found strong asymmetries with respect to the order in which graphene layers are traversed by the external charged particle that are manifested in the angular distributions of TR in the half-spaces defined by the DLG, as well as in the amounts of energy deposited in individual graphene layers, which mostly goes into the excitation of two HDPP modes. Those asymmetries were found to be accentuated by increasing interlayer distance and by increasing asymmetry between the doping densities of the two graphene layers in a DLG [14]. In this work, we add the number N of layers as a critically important parameter for all MLG structures, and investigate how the above mentioned physical observations change with N in the range $1 \leqslant N \leqslant 5$ for equally doped graphene layers with a broad range of interlayer distances.

In the following section we briefly outline the elements of theoretical modeling, while referring to [13, 14] for more details, and in section 3 we discuss several representative results of our calculations, which will enable us to draw conclusions about MLG in the section 4.

Unless otherwise stated, Gaussian units of electrodynamics are used throughout the paper [42].

2. Theory

We first provide brief outline of a theoretical framework for obtaining various energy loss distributions for a general MLG structure, which was detailed in [14]. Those distributions take the in-plane, 2D conductivity for each graphene layer as input functions, which may be available in an analytical form from empirical models or can be obtained in tabulated form from *ab initio* calculations [39]. We then discuss a range of parameters, which renders Drude model an adequate description of graphene's conductivity for the use in this work [5].

2.1. Energy loss distributions

We consider an MLG structure consisting of N parallel graphene sheets of large area placed in the planes $z = z_l$ with $l = 1, 2, \ldots, N$ of a three-dimensional (3D) Cartesian system with coordinates $\mathbf{R} = \{x, y, z\}$. An external point charge Ze is assumed to move along the z-axis with constant speed v. Performing the two-dimensional (2D) spatial Fourier transform ($\mathbf{r} = \{x, y\} \rightarrow \mathbf{k} = \{k_x, k_y\}$) and a Fourier transform with respect to time ($t \rightarrow \omega$), one may express the external charge current density as $\mathbf{J}_{\rm ext}(\mathbf{k}, z, \omega) = Ze\, {\rm e}^{{\rm i}z\frac{\omega}{v}}\,\hat{\mathbf{z}}$, where $\hat{\mathbf{z}}$ is a unit vector in the direction of the z-axis. Due to dynamic polarization of charge carriers in graphene layers by the external electromagnetic fields, each layer supports the in-plane current density, $\mathbf{j}_l(\mathbf{k}, \omega)$, which yields the total induced current density as $\mathbf{J}_{\rm ind}(\mathbf{k}, z, \omega) = \sum_{l=1}^{N} \delta(z - z_l)\mathbf{j}_l(\mathbf{k}, \omega)$. We assume that the lth graphene layer is characterized by an equilibrium density of charge carriers, n_l, giving rise to an in-plane, scalar conductivity $\sigma_l(k, \omega)$, which is independent of the conductivities of other layers, and is generally dependent on both the wavenumber $k = \sqrt{k_x^2 + k_y^2}$ and frequency ω. Then, the polarization current in that layer may be expressed via the Ohm's law as $\mathbf{j}_l(\mathbf{k}, \omega) = \sigma_l(k, \omega)\mathbf{E}_{\rm tot}^{\parallel}(\mathbf{k}, z_l, \omega)$, where $\mathbf{E}_{\rm tot}^{\parallel}(\mathbf{k}, z_l, \omega)$ is the tangential, or the in-plane component of the total electric field, $\mathbf{E}_{\rm tot}(\mathbf{k}, {\rm z}, \omega)$, evaluated at $z = z_l$.

As discussed in [14], the key step in obtaining a self-consistent solution of the problem at hand is a system of N equations for the longitudinal components of the in-plane electric fields, $E_l \equiv \hat{\mathbf{k}} \cdot \mathbf{E}_{\rm tot}^{\parallel}(\mathbf{k}, z_l, \omega)$, where $\hat{\mathbf{k}} = \mathbf{k}/k$, which is given by

$$\left(1 + \frac{2\pi {\rm i}}{\omega} q\, \sigma_l\right) E_l + \frac{2\pi {\rm i}}{\omega} q \sum_{l'=1, l' \neq l}^{N} \sigma_{l'} {\rm e}^{-q|z_l - z_{l'}|} E_{l'} = \mathcal{A}\, {\rm e}^{{\rm i}z_l\frac{\omega}{v}}. \tag{1}$$

Here,

$$q(k, \omega) = \begin{cases} \sqrt{k^2 - (\omega/c)^2}, & |\omega| < ck, \\ -{\rm i}\,{\rm sign}(\omega)\sqrt{(\omega/c)^2 - k^2}, & |\omega| > ck, \end{cases} \tag{2}$$

whereas

$$\mathcal{A} = {\rm i}k\frac{Ze}{v}\frac{4\pi}{\frac{\omega^2}{v^2} - \frac{\omega^2}{c^2} + k^2}. \tag{3}$$

Using the solution of the system equation (1) in the Ohm's law for each graphene layer enables us to find the induced current density in those layers and ultimately obtain the induced electric and magnetic fields, $\mathbf{E}_{\rm ind}(\mathbf{k}, {\rm z}, \omega)$ and $\mathbf{H}_{\rm ind}(\mathbf{k}, {\rm z}, \omega)$, throughout the structure, given in [14]. Moreover, the eigenvalues of the system in equation (1) yield N eigenfrequencies $\omega_j(k)$, with $j = 1, 2, \ldots, N$, of the HDPP modes, satisfying $0 < \omega_j(k) < ck$.

Physically, one expects that the energy loss of the external charged particle is distributed into TR and ohmic loss, describing the energy emitted in the form of electromagnetic radiation in the far field region and the energy going into electronic excitations that remain confined to individual graphene layers, respectively. It should be mentioned that, by adopting the Drude model when these processes take place in the THz frequency range, the ohmic energy loss only involves excitation of the HDPP modes, followed by the dissipation of their energy into Joule heat. In our previous work, we used physical definitions for the total energy loss of the external charged particle, $W_{\rm ext}$, ohmic energy loss in graphene layers, $W_{\rm ohm}$, and the radiation energy loss, $W_{\rm rad}$, and verified that the energy balance of the system composed of the incident

particle and the MLG is explicitly upheld in the form $W_{\rm ext} = W_{\rm ohm} + W_{\rm rad}$ for an SLG [13] and a DLG [14]. In the following we give the corresponding expressions to extend this analysis for an arbitrary number of layers.

Invoking the parity properties of the Fourier transformed quantities, we may express the energy loss for each of those channels as the integrals

$$W_{\rm L} \equiv \iint {\rm d}^2\mathbf{k} \int_0^{+\infty} {\rm d}\omega\ \omega\ F_{\rm L}(k,\ \omega) \equiv \hbar^2 \int_0^{\infty} {\rm d}\omega\ \omega\ P_{\rm L}(\omega), \tag{4}$$

where L = ext, ohm, rad. The above expressions define the corresponding joint probability densities, $F_{\rm L}(k,\ \omega)$, associated with the transfer of energy $\hbar\omega \geqslant 0$ and the transfer of in-plane momentum $\hbar\mathbf{k}$ from the incident electron to graphene layers, as well as the corresponding integrated probability densities, $P_{\rm L}(\omega)$. Specifically, we find for the energy loss of the external charged particle,

$$F_{\rm ext}(k,\ \omega) = -\frac{1}{4\pi^3\omega}\Re\left\{\int_{-\infty}^{+\infty} {\rm d}z\ \mathbf{J}_{\rm ext}(\mathbf{k},\ z,\ \omega)\cdot \mathbf{E}^*_{\rm ind}(\mathbf{k},\ z,\ \omega)\right\} \tag{5}$$

$$= \frac{1}{4\pi^3\omega}\sum_{l=1}^{N}\Re\{\sigma_l E_l \mathcal{A}\ {\rm e}^{-{\rm i}z_l\frac{\omega}{v}}\}. \tag{6}$$

Using the definition of the total ohmic loss we obtain a layer-wise decomposition in the form

$$F_{\rm ohm}(k,\ \omega) = \frac{1}{4\pi^3\omega}\Re\left\{\int_{-\infty}^{+\infty} {\rm d}z\ \mathbf{J}_{\rm ind}(\mathbf{k},\ z,\ \omega)\cdot \mathbf{E}^*_{\rm tot}(\mathbf{k},\ z,\ \omega)\right\} \tag{7}$$

$$= \sum_{l=1}^{N} F_{{\rm ohm},l}(k,\ \omega), \tag{8}$$

where

$$F_{{\rm ohm},l}(k,\ \omega) = \frac{1}{4\pi^3\omega}\ |E_l|^2\ \Re\{\sigma_l\} \tag{9}$$

is the ohmic energy loss contained in the lth graphene layer. Similarly, the integrated ohmic loss may also be decomposed into contributions from separate layers, $P_{\rm ohm}(\omega) = \sum_{l=1}^{N} P_{{\rm ohm},l}(\omega)$.

The joint probability density of the radiation energy losses satisfying $\omega > ck$, which occur in the upper and lower half-spaces, may be obtained from the induced Poynting vector as

$$F^{\uparrow\downarrow}_{\rm rad}(k,\ \omega) = \frac{\pm c}{\omega(2\pi)^4}\lim_{z\to\pm\infty}\Re\{\hat{\mathbf{z}}\cdot[\mathbf{E}_{\rm ind}(k,\ z,\ \omega) \times \mathbf{H}^*_{\rm ind}(k,\ z,\ \omega)]\} \tag{10}$$

$$= \frac{\kappa}{\omega^2(2\pi)^2}\sum_{l=1}^{N}\sum_{l'=1}^{N}\Re\{\sigma_l\ \sigma^*_{l'}{\rm e}^{\mp{\rm i}\kappa(z_l - z_{l'})}E_l\ E^*_{l'}\}, \tag{11}$$

where $\kappa \equiv \sqrt{(\omega/c)^2 - k^2}$. The total joint probability density for the radiation energy loss, $F_{\rm rad}(k,\ \omega) = F^{\uparrow}_{\rm rad}(k,\ \omega) + F^{\downarrow}_{\rm rad}(k,\ \omega)$, may be related to the spectral angular distribution of radiation, $\mathcal{S}(\theta,\ \omega)$, where θ is the angle of the emitted radiation with respect to the direction of motion of the external charged particle (z axis), via the relation

$$W_{\rm rad} \equiv \iint {\rm d}^2\mathbf{k} \int_0^{+\infty} {\rm d}\omega\ \omega\ F_{\rm rad}(k,\ \omega) \equiv \iint {\rm d}^2\hat{\Omega} \int_0^{\infty} {\rm d}\omega\ \mathcal{S}(\theta,\ \omega). \tag{12}$$

In the above equation, we used spherical coordinates to express $\mathbf{k} = \{k_x,\ k_y\} = \frac{\omega}{c}\sin\theta\{\cos\phi,\ \sin\phi\}$ and define the differential solid angle ${\rm d}^2\hat{\Omega} = \sin\theta\ {\rm d}\theta\ {\rm d}\phi$, with $0 \leqslant \theta \leqslant \pi$ and $0 \leqslant \phi < 2\pi$. In a similar manner to the ohmic energy loss, we may express the directional decomposition of the total integrated radiation loss as $P_{\rm rad}(\omega) = P^{\uparrow}_{\rm rad}(\omega) + P^{\downarrow}_{\rm rad}(\omega)$, with the integrated radiation loss in the upper/lower half-space defined by

$$P^{\uparrow\downarrow}_{\rm rad}(\omega) = \frac{1}{\hbar^2}\iint {\rm d}^2\mathbf{k}\ F^{\uparrow\downarrow}_{\rm rad}(k,\ \omega) = \frac{1}{\hbar^2\omega}\iint\limits_{\vee,\wedge} {\rm d}^2\hat{\Omega}\ \mathcal{S}(\theta,\ \omega), \tag{13}$$

where the last integral goes over $0 \leqslant \theta \leqslant \pi/2$ in the upper ($\vee$) and $\pi/2 \leqslant \theta \leqslant \pi$ in the lower ($\wedge$) half-space.

2.2. Conductivity model

We assume that graphene layers within an MLG are electronically decoupled from each other, i.e., they are spatially separated far enough that the electronic band structure of each layer is unaffected by the presence of other layers. Therefore, we adopt the Drude model for the conductivity of each layer, which was shown to be an adequate description of its dynamic polarization in the THz range of frequencies [5, 39]. This model is accurate enough for $k \ll \omega/v_F \ll k_F$, where $v_F \approx c/300$ is the Fermi speed in graphene and $k_F = \sqrt{\pi|n|}$ is the Fermi wavenumber in a graphene layer doped with the charge carrier density n [4]. In the THz range, it is convenient to work with nondimensionalized wavenumber and frequency, defined as $\overline{k} = k/k_c$ and $\overline{\omega} = \omega/\omega_c$, respectively, where $k_c = e^2 v_F k_F/(\hbar c^2)$ and $\omega_c = ck_c$ [13]. We note that for the doping density of $|n| = 2.36 \times 10^{13}$ cm^{-2}, with the corresponding Fermi energy of $\varepsilon_F = \hbar v_F k_F \approx 0.57$ eV that is easily achieved in experiments with MLG, one obtains $\lambda_c = 2\pi/k_c \approx 300\,\mu$m and $\nu_c = \omega_c/(2\pi) \approx 1$ THz. Thus, defining the reduced conductivity by $\overline{\sigma} = \sigma/c$, the Drude model gives

$$\overline{\sigma}(\overline{\omega}) = \frac{\rm i}{\pi}\frac{1}{\overline{\omega} + {\rm i}\overline{\gamma}}, \tag{14}$$

where $\overline{\gamma} = \gamma/\omega_c$ is the reduced damping rate.

Clearly, the Drude model neglects nonlocal effects in the graphene conductivity, which may become critical for theoretical modeling of the quasi-acoustic HDPP modes in an MLG [31–33, 35]. Namely, the lowest-lying of those modes may be pushed close to the boundary line $\omega = v_F{\rm k}$ of the continuum of the low-energy, single electron excitations within graphene's π electron bands [4]. Defining the reduced distance between graphene layers as $\overline{d} = k_c d$ (assuming equally spaced layers), one may use equation (9) in [32] to show that the condition $\overline{d} \gg (v_F/c)^2$ guarantees that the dispersions of the lowest-lying HDPPs are well above the line $\omega = v_F k$, thereby rendering the Drude model adequate for all

HDPP modes in an MLG. In order to test the role of nonlocal effects, we have performed calculations using a wavenumber dependent conductivity based on the random-phase approximation given in [43]. We have found no difference in comparison with the results obtained from the Drude model in equation (14), even down to $\overline{d} = 10^{-5}$. We adopt here the range of interlayer distances $10^{-3} \leqslant \overline{d} \leqslant 1$, corresponding to the physical distances of 48 nm $\lesssim d \lesssim$ 48 μm for the doping density of $|n| = 2.36 \times 10^{13}$ cm^{-2}. We note that, even for the shortest distance of $d = 48$ nm considered in this work, which is comparable to distances used in the experiments in [18, 22], one may safely assume that graphene layers are electronically decoupled and their only interaction is due to the electromagnetic fields.

It should be mentioned that theoretical modeling of optical experiments using MLG at THz frequencies often invokes an approximation that the conductivity of N equally doped graphene layers is given by $\sigma_N(\omega) = N\sigma(\omega)$, where $\sigma(\omega)$ is the optical conductivity of an SLG [18, 22, 24]. This approximation is expected to work well if the interlayer distances are not too large, so that the MLG may be considered as optically thin, but also not too small, so that the graphene layers are electronically decoupled. The validity of this approximation was confirmed in experiments using plasmonic devices with two graphene layers separated by a 80 nm polymer layer [22], stacks of up to $N = 5$ graphene layers separated by 20 nm thick spacers [18], periodic lattices of graphene nanoribbons in two parallel planes a distance 1 nm apart [23], and even stacks of randomly oriented graphene layers with $d \sim 0.3$ nm [24]. Accordingly, we shall verify the range of applicability of the above approximation for optically thin MLG in the present context by using an analytical result obtained in [13] for the integrated ohmic energy loss in an SLG, $P_{\rm ohm}^{\rm SLG}[\sigma(\omega), \omega]$, where the conductivity of an SLG is replaced by $\sigma_N(\omega) = N\sigma(\omega)$.

3. Results and discussion

In our previous work we have shown that there are strong effects of variations in the charged particle speed v and the damping rate γ on both the ohmic and radiation energy losses in an SLG [13] and a DLG [14]. Moreover, we have found strong effects due to differences in doping densities of graphene layers in a DLG [14]. However, in order to decrease the size of the parameter space in this work, we keep the reduced particle speed fixed at $\beta = v/c = 0.5$ (corresponding to a typical electron energy in a TEM) and the reduced damping rate fixed at $\overline{\gamma} = 0.05$, while assuming that all graphene layers are doped with equal densities. For the same reason, we assume equal spacing d between the nearest graphene layers in an MLG. Thus, with the conductivity of each layer being described by equation (14), we concentrate on the effects of variations in the number of layers N and the interlayer distance d for the energy loss and radiation spectra when a fast charged particle traverses an MLG.

In figure 1, we use reduced units to show the joint probability densities of the total ohmic energy loss, $\overline{F}_{\rm ohm}(\overline{k}, \overline{\omega}) = F_{\rm ohm}(\overline{k}, \overline{\omega})/F_c$ (panel (a)), and the total radiation energy loss, $\overline{F}_{\rm rad}(\overline{k}, \overline{\omega}) = F_{\rm rad}(\overline{k}, \overline{\omega})/F_c$ (panel (b)), where $F_c = 4(Ze)^2/(\pi\omega_c^2 k_c)$, as well as the dispersion curves for three HDPP modes, $\overline{\omega} = \overline{\omega}_j(\overline{k})$, with $j = 1$, 2 and 3 (panel (c)), for a TLG structure with $\overline{d} = 0.1$. Besides the exact dispersion curves, for the sake of comparison we also show in figure 1(c) three approximations to the exact dispersion curves, $\overline{\omega} = \overline{\omega}_j^{\rm appr}(\overline{k})$, as well as the DPP dispersion curve for an SLG with $\overline{\omega}_{\rm SLG}(\overline{k}) = \sqrt{2(-1 + \sqrt{1 + \overline{k}^2})}$.

By comparison with the panel (c), it is clear that the main contribution to the ohmic energy loss in panel (a) of figure 1 occurs predominantly in the regions close to the three HDPP dispersion curves. Those regions exhibit different amounts of broadening, such that the largest width occurs along the middle dispersion curve, $\overline{\omega} = \overline{\omega}_2(\overline{k})$, and the smallest width occurs along the lowest dispersion curve, $\overline{\omega} = \overline{\omega}_1(\overline{k})$. One notices that the three broadened curves merge in figure 1(a), giving rise to a relatively broad and structureless background of ohmic energy loss in a region of very small $\overline{\omega}$ and $\overline{k}$ values, which is a consequence of finite damping rate that governs dissipative processes at low frequencies. It should be stressed that, even though part of this background extends above the light line, $\overline{\omega} > \overline{k}$, the associated processes do not give rise to any radiation, but rather produce Joule heat that remains in graphene. On the other hand, we display in the panel (b) of figure 1 the energy loss density due to the TR, which is seen to be broadly distributed in a region that is located strictly above the light line.

In the panel (c) of figure 1, one notices that all three dispersion curves lie below the light line, $\overline{\omega} = \overline{k}$, and that the highest dispersion exhibits a transition to the $\overline{\omega}_3 \propto \sqrt{\overline{k}}$ form, whereas the two lower lying curves exhibit quasi-acoustic dispersions. Besides the dispersion curves with the exact eigenfrequencies, $\overline{\omega}_j(\overline{k})$, we also show in figure 1(c) their corresponding long wavelength approximations with frequencies $\overline{\omega}_j^{\rm appr}(\overline{k})$ for $j = 1$, 2, 3. The highest-lying dispersion is approximated with $\overline{\omega}_3^{\rm appr}(\overline{k})$, which is evaluated by making the assumption that an N-layer MLG may be treated as an SLG with an effective conductivity given by $\overline{\sigma}_N(\overline{\omega}) = N\overline{\sigma}(\overline{\omega})$. This assumption yields a dispersion relation with the approximate eigenfrequency $\overline{\omega}_N^{\rm appr}(\overline{k}) = N\sqrt{2\left(-1 + \sqrt{1 + \frac{\overline{k}^2}{N^2}}\right)}$, shown for $N = 3$ by the dotted line in figure 1(c). This relation reproduces well the exact dispersion curve $\overline{\omega} = \overline{\omega}_3(\overline{k})$ for sufficiently long wavelengths, but deviations are already observed for $\overline{k} \gtrsim 2$. On the other hand, the two lower-lying dispersion curves that behave as quasi-acoustic modes at long wavelengths, may be approximated to the leading order in $\overline{k}$ by the eigenfrequencies $\overline{\omega}_2^{\rm appr}(\overline{k}) = \overline{k}\sqrt{4\overline{d}/(1 + 4\overline{d})}$ and $\overline{\omega}_1^{\rm appr}(\overline{k}) = \overline{k}\sqrt{4\overline{d}/(3 + 4\overline{d})}$, which are obtained from equation (1) in the limit $\overline{k} \to 0$. Similarly to $\overline{\omega}_3^{\rm appr}(\overline{k})$, one notices in figure 1(c) that the lower-lying approximations $\overline{\omega}_{1,2}^{\rm appr}(\overline{k})$ are quite close to the corresponding exact modes $\overline{\omega}_{1,2}(\overline{k})$ for wavenumbers $\overline{k} \lesssim 1$.

For further reference, it is worthwhile commenting on the behavior of the exact dispersion curves with $\overline{\omega}_j(\overline{k})$ in the

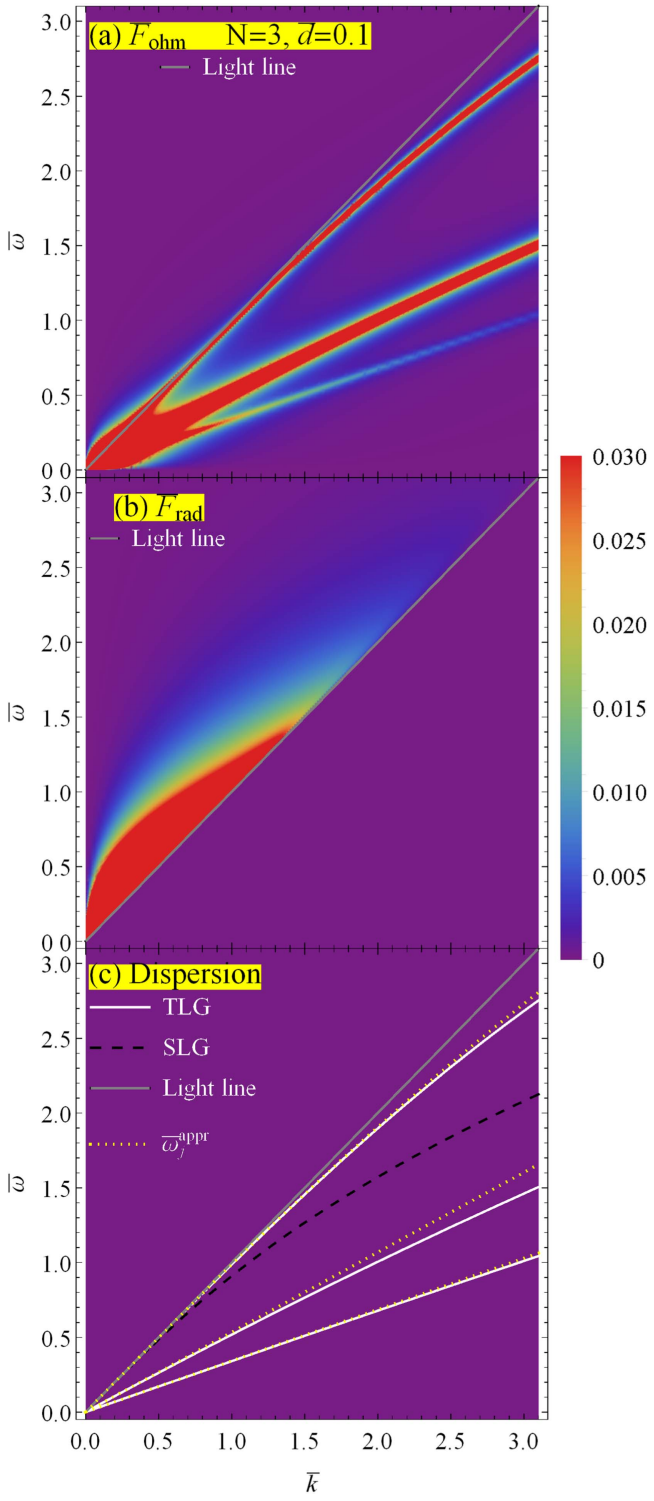

Figure 1. The total ohmic energy loss density, $\bar{F}_{ohm} = F_{ohm}/F_c$ (panel (a)), and the total radiative energy loss density, $\bar{F}_{rad} = F_{rad}/F_c$ (panel (b)), are displayed in reduced units with $F_c = 4(Ze)^2/(\pi\omega_c^2 k_c)$, as functions of the reduced wavenumber $\bar{k} = k/k_c$ and the reduced frequency $\bar{\omega} = \omega/\omega_c$, for a three-layer graphene with reduced interlayer distance $\bar{d} = k_c d = 0.1$. Panel (c) displays with white solid lines the dispersion curves for three hybridized Dirac plasmon polariton modes, $\bar{\omega} = \bar{\omega}_j(\bar{k})$ for $j = 1, 2, 3$, along with the corresponding long-wavelength approximations (white dotted lines), a dispersion curve for single-layer graphene (black dashed line), and the light line $\bar{\omega} = \bar{k}$ (gray solid line).

range of large $\bar{k}$ values, well beyond those shown in figure 1(c). While those curves are seen in figure 1(c) to diverge with increasing $\bar{k}$, one can see in figure S1 of the supplementary material (SM) available online at stacks.iop.org/NANO/29/225201/mmedia that they start converging for $\bar{k} \sim 15$. For still larger wavenumbers, say $\bar{k} \gtrsim 30$, all three dispersion curves are found in figure S1 to approach the dispersion relation of a SLG, with an eigenfrequency that is well approximated at such short wavelengths by its non-retarded limit, $\bar{\omega}_{SLG} = \sqrt{2\bar{k}}$. Thus, we expect that hybridization among the DPP modes in a TLG with $\bar{d} = 0.1$ becomes negligible at frequencies $\bar{\omega} \gtrsim 10$.

In figure 2, we show a decomposition of the total ohmic energy loss from figure 1(a), $\bar{F}_{ohm}(\bar{k}, \bar{\omega}) = \sum_{l=1}^{3} \bar{F}_{ohm,l}(\bar{k}, \bar{\omega})$, with contributions to the top ($l = 3$, panel (a)), middle ($l = 2$, panel (b)), and the bottom ($l = 1$, panel (c)) graphene layers. In the insets to the panels in figure 2, we display the cross sections of the corresponding ohmic energy losses $\bar{F}_{ohm,l}(\bar{k}, \bar{\omega})$ for $\bar{k} = 0.5$, along with three vertical bars showing the positions of the corresponding HDPP mode frequencies $\bar{\omega}_j(\bar{k})$, evaluated from figure 1(c) at $\bar{k} = 0.5$ for $j = 1, 2, 3$. It is remarkable that the widths of the peak regions in the spectra $\bar{F}_{ohm,l}(\bar{k}, \bar{\omega})$ corresponding to the three HDPP dispersions, are differently distributed in different graphene layers. So, for example, in the panel (a) we see that in the top layer ($l = 3$) the widest contribution occurs along the middle dispersion curve $\bar{\omega}_2$, a somewhat narrower contribution occurs along the highest dispersion curve $\bar{\omega}_3$, and the narrowest contribution occurs along the lowest lying dispersion curve $\bar{\omega}_1$. A similar distribution of widths is seen in the panel (c) for the bottom layer ($l = 1$), with two important differences: the contribution in the region above the light line is more abundant than in the top layer for small $\bar{\omega}$ and $\bar{k}$ values and, more interestingly, there exists a *dip* near the position of the dispersion curve $\bar{\omega} = \bar{\omega}_1(k)$, which is clearly discernible on the nearby diffuse background for small $\bar{\omega}$ and $\bar{k}$ values below the light line. A closer inspection of that dip in the inset to the panel (c) shows that the contribution of the lowest lying HDPP mode to ohmic energy losses in the bottom graphene layer has the characteristics of a Fano resonance [26, 34, 44]. This may be tentatively explained by an assertion that the resonance due to the HDPP mode with $\bar{\omega}_2$ is broad enough and the resonance due to the HDPP mode with $\bar{\omega}_1$ narrow enough, so that destructive interferences between them cause diminishing ohmic losses at frequencies $\bar{\omega}_1(\bar{k}) \lesssim \bar{\omega} < \bar{\omega}_2(\bar{k})$ in the bottom graphene layer. It should also be noticed in the panel (c) that the strongly asymmetric shape of the Fano resonance near $\bar{\omega} = \bar{\omega}_1(\bar{k})$ in the bottom layer effectively pushes the contribution of the ohmic loss in that layer towards somewhat lower frequencies than $\bar{\omega}_1$ when compared to the regions below the broadened resonances along the dispersion $\bar{\omega} = \bar{\omega}_1(\bar{k})$ in the middle and top layers. On the other hand, the reason for the lack of a Fano shape in the top graphene layer, as observed in the inset to the panel (a), is not obvious, but may be guessed to be due to insufficient difference between the widths of resonances corresponding to the HDPP modes with $\bar{\omega}_1$ and $\bar{\omega}_2$ in that layer. In any case, those two

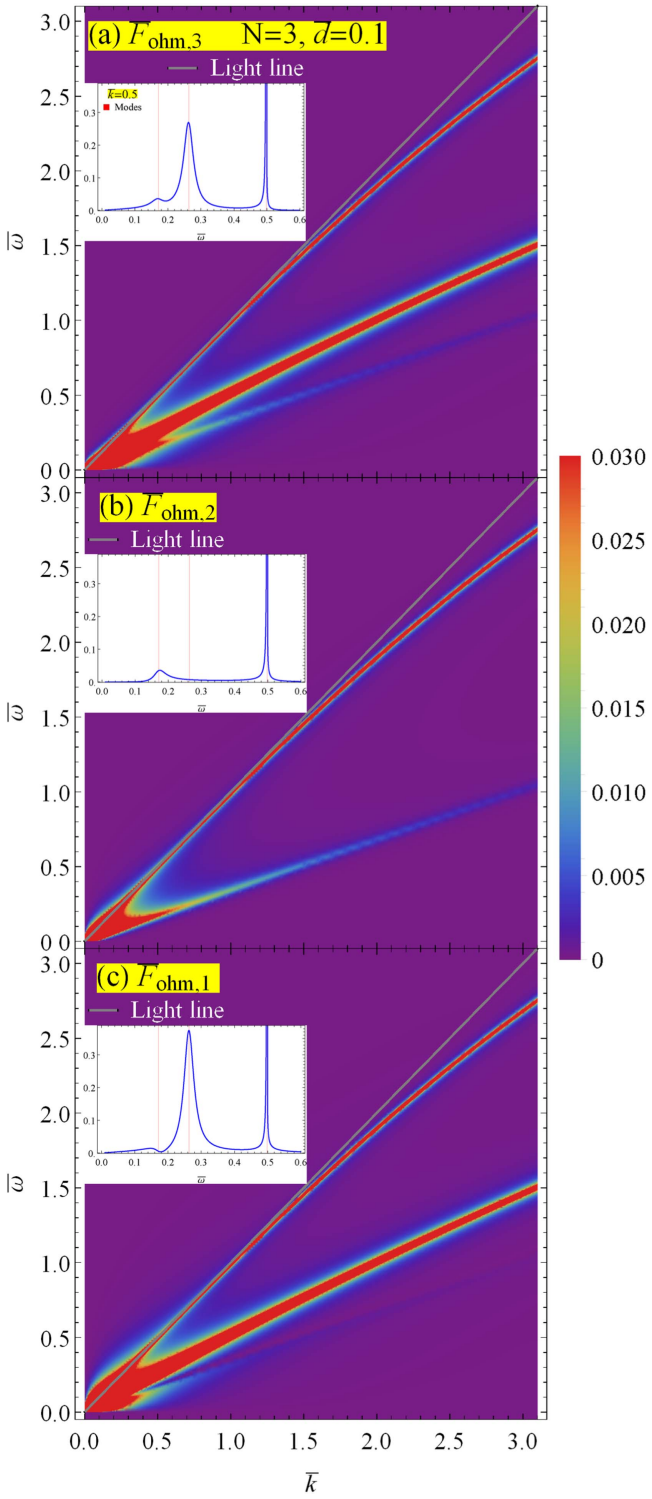

Figure 2. A decomposition of the ohmic energy loss, $\overline{F}_{\mathrm{ohm},l}(\overline{k},\overline{\omega}) = F_{\mathrm{ohm},l}(\overline{k},\overline{\omega})/F_c$, is displayed in reduced units with $F_c = 4(Ze)^2/(\pi\omega_c^2 k_c)$, as a function of the reduced wavenumber $\overline{k} = k/k_c$ and the reduced frequency $\overline{\omega} = \omega/\omega_c$, for a three-layer graphene with reduced interlayer distance $\overline{d} = k_c d = 0.1$. Contributions to the top ($l = 3$), middle ($l = 2$), and bottom ($l = 1$) layers are shown in the panels (a), (b) and (c), respectively. The insets display the corresponding cross-sections of $\overline{F}_{\mathrm{ohm},l}(\overline{k},\overline{\omega})$ for $\overline{k} = 0.5$, with the red vertical bars showing the values of the hybridized Dirac plasmon polariton eigenfrequencies, $\overline{\omega}_j(\overline{k})$ for $j = 1, 2, 3$, evaluated from figure 1(c) at $\overline{k} = 0.5$.

differences between the ohmic energy loss distributions in the top and bottom layers signal an asymmetry with respect to the order in which graphene layers are traversed by the external charged particle, pointing to the retardation effects as their common cause.

However, the most striking behavior of the three HDPP modes is observed in the panel (b) of figure 2 for the middle graphene layer ($l = 2$), where the ohmic energy loss in the region corresponding to the mode with the middle dispersion curve $\overline{\omega}_2$ is completely missing, whereas the widths of the resonant modes with $\overline{\omega}_1$ and $\overline{\omega}_3$ are similar to the corresponding widths in the top layer in the panel (a). This may be tentatively explained by the nature of charge carrier oscillations in the three graphene layers, which give rise to the HDPP modes with eigenfrequencies $\overline{\omega}_1$, $\overline{\omega}_2$ and $\overline{\omega}_3$ (see, e.g., figure S1(b) in [23]). Namely, the mode with the highest-lying $\overline{\omega}_3$ is characterized by an in-phase oscillations of charges in all three layers, whereas the mode with the lowest-lying $\overline{\omega}_1$ is characterized by an in-phase oscillations of charges in the outer layers and the out-of-phase oscillations of charges in the middle layer. On the other hand, the mode with the middle eigenfrequency $\overline{\omega}_2$ is characterized by the out-of-phase oscillations of charges in the outer layers, whereas the charges in the middle layer oscillate in phase with charges in either the upper or in the lower graphene layer. Owing to this double degeneracy of charge configurations at the middle eigenfrequency in a symmetric structure of equally spaced and equally doped graphene layers in a TLG, one may surmise that, on average, there is no charge carrier polarization in the middle layer for the HDPP mode with $\overline{\omega}_2$.

In figure 3, we show the angular distributions of the spectral density for TR in reduced units, $\overline{\mathcal{S}}(\theta,\overline{\omega}) = \mathcal{S}/\mathcal{S}_c$ with $\mathcal{S}_c = (Ze)^2/c$, for a TLG system with (a) $\overline{d} = 0.1$ and (b) $\overline{d} = 1$. One notices in the panel (a) that the angular patterns in the upper and lower half-spaces are largely similar in shape, but slight asymmetry starts appearing for frequencies $\overline{\omega} \gtrsim 1$. On the other hand, one sees in the panel (b) that an increase of the interlayer separation to $\overline{d} = 1$ gives rise to an asymmetry between the angular patterns emitted in the upper and lower half-spaces already for $\overline{\omega} \gtrsim 0.1$, which becomes quite strong with increasing frequency. A similar effect was observed for a DLG in [14], albeit for somewhat larger interlayer separations. One may surmise that, for the MLG systems, which may not be considered optically thin, as is likely the case in figure 3(b), there are strong interferences in the TR emission patterns due to retardation effects. These interferences can be ascribed to products of the oscillatory factors $\exp[\mp \mathrm{i}\kappa(z_l - z_{l'})]$ and $\exp\left[\mp \mathrm{i}\frac{\omega}{v}(z_l - z_{l'})\right]$ in equation (11), which give rise to the observed asymmetry in the radiation energy loss for increasing $\overline{\omega}\overline{d}$ values.

Figure 4 shows several integrated probability densities in reduced units, $\overline{P}(\overline{\omega}) = P/P_c$ with $P_c = \frac{4}{\pi}\frac{1}{\varepsilon_F}$, for a TLG system with (a) $\overline{d} = 0.1$ (studied in figure 1) and (b) $\overline{d} = 1$. In addition to the total ohmic energy loss and the total radiation energy loss, we show their decompositions into the contributions to different graphene layers, $\overline{P}_{\mathrm{ohm}} = \sum_{l=1}^{3} \overline{P}_{\mathrm{ohm},l}$,

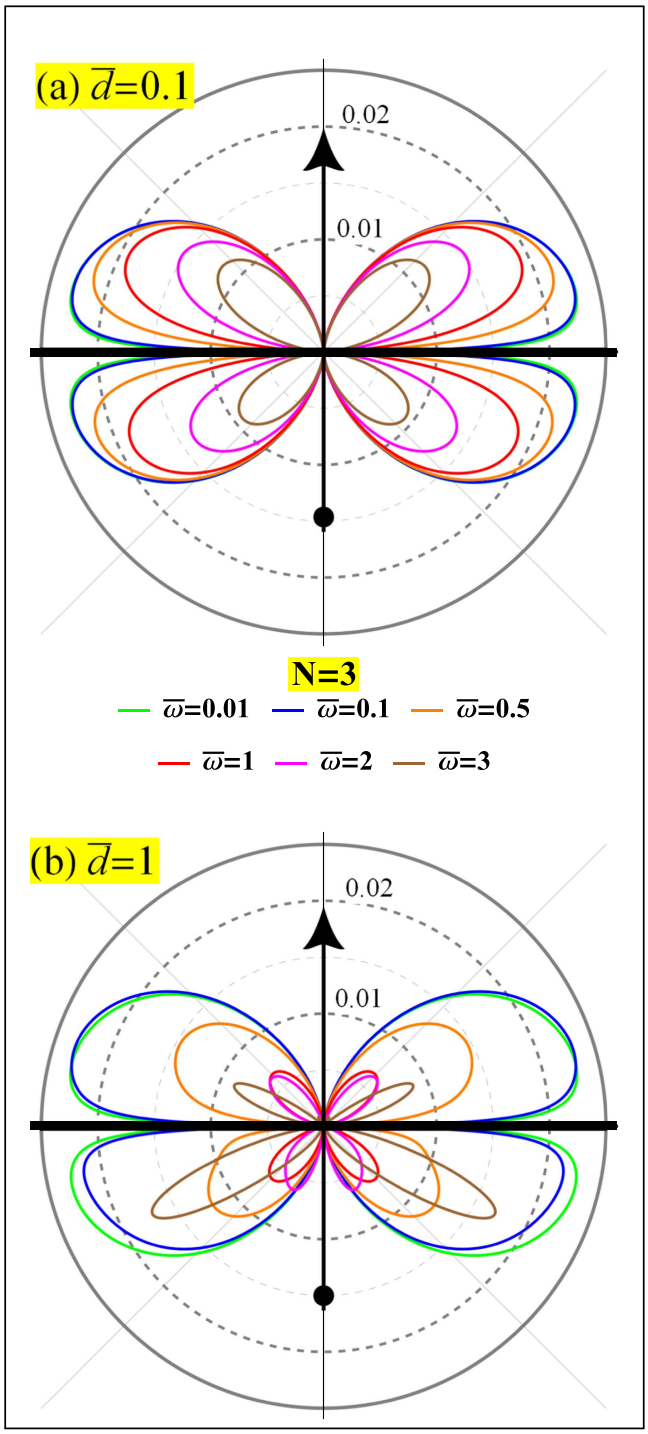

Figure 3. Angular distribution of the spectral density for transition radiation, $\overline{\mathcal{S}}(\theta, \overline{\omega}) = \mathcal{S}/\mathcal{S}_c$, shown in reduced units with $\mathcal{S}_c = (Ze)^2/c$, for a three-layer graphene with reduced interlayer distances: (a) $\overline{d} = 0.1$ and (b) $\overline{d} = 1$, for several values of the reduced frequency $\overline{\omega}$.

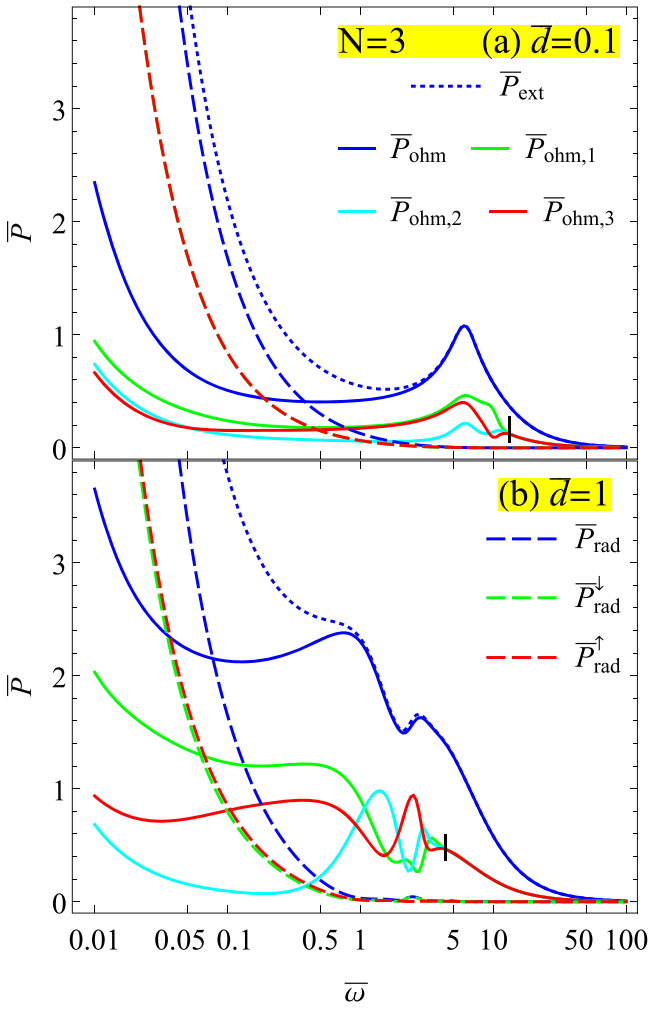

Figure 4. Integrated probability density, $\overline{P}(\overline{\omega}) = P(\overline{\omega})/P_c$, shown in reduced units with $P_c = \frac{4}{\pi}\frac{1}{\varepsilon_F}$, for a three-layer graphene with reduced interlayer distances: (a) $\overline{d} = 0.1$ and (b) $\overline{d} = 1$. In addition to the total ohmic energy loss, $\overline{P}_{ohm}(\overline{\omega})$ (blue solid lines), and the total radiation energy loss, $\overline{P}_{rad}(\overline{\omega})$ (blue dashed lines), we show their decompositions into different graphene layers, $\overline{P}_{ohm,l}(\overline{\omega})$ with $l = 1$, 2, 3 for the bottom, middle and top layers (solid lines), and radiation emitted in the upper/lower half-spaces, $\overline{P}^{\uparrow,\downarrow}_{rad}(\overline{\omega})$ (dashed lines), respectively. Also shown by dotted blue lines is the total energy loss of the external charged particle from equation (6), confirming the conservation of energy as $\overline{P}_{ext}(\overline{\omega}) = \overline{P}_{ohm}(\overline{\omega}) + \overline{P}_{rad}(\overline{\omega})$. The black vertical bars at (a) $\overline{\omega} = 13.3$ and (b) $\overline{\omega} = 4.2$ indicate frequencies below which $\overline{P}_{ohm,l}(\overline{\omega})$ exhibit large differences.

and contributions to the upper and lower half-spaces, $\overline{P}_{rad} = \overline{P}^{\uparrow}_{rad} + \overline{P}^{\downarrow}_{rad}$, respectively. We also display a result for the total energy loss of the external charged particle evaluated from the definition in equation (6), showing the conservation of energy in the form $\overline{P}_{ext}(\overline{\omega}) = \overline{P}_{ohm}(\overline{\omega}) + \overline{P}_{rad}(\overline{\omega})$.

One notices in the panel (a) of figure 4 that the radiation contributions to the upper and lower half-spaces, $\overline{P}^{\uparrow}_{rad}$ and $\overline{P}^{\downarrow}_{rad}$, are practically identical for $\overline{d} = 0.1$ at all frequencies, which is not surprising given the similarity of the angular patterns in figure 3(a). On the other hand, the two radiation contributions in the panel (b) of figure 4 are quite close to each other, with somewhat higher values of the radiation emitted in the upper than in the lower half-space, $\overline{P}^{\uparrow}_{rad} > \overline{P}^{\downarrow}_{rad}$ for $\overline{\omega} < 1$. However, it is surprising that, for the case of a TLG with $\overline{d} = 1$, which is not optically thin, the strong asymmetry between the angular patterns observed in figure 3(b) at frequencies $\overline{\omega} > 1$, does not give rise to any detectable asymmetry between $\overline{P}^{\uparrow}_{rad}$ and $\overline{P}^{\downarrow}_{rad}$ in figure 4(b) in the same range of frequencies, except for a small 'bump' at $\overline{\omega} \approx 2.5$. It should be noted, however, that the radiation

energy losses are heavily suppressed for frequencies $\overline{\omega} > 1$ in figure 4, but they give a dominant contribution to the total energy losses of the external charged particle at frequencies $\overline{\omega} < 0.5$ and $\overline{\omega} < 0.1$ in the panels (a) and (b), respectively. It is remarkable that the radiation energy losses at those frequencies show no significant differences when the interlayer distance changes from $\overline{d} = 0.1$ to $\overline{d} = 1$ in going from the panel (a) to (b) in figure 4. This may be rationalized by asserting that only charge carrier oscillations in the *outer* graphene layers give rise to the emission of electromagnetic energy in the far field regions, whereas the integration over the angles in equation (13) causes a massive cancelation in the Poynting vector for radiative components of the electromagnetic fields due to destructive interferences in the regions between graphene layers.

In view of the above discussed similarity between the radiation contributions $\overline{P}^{\uparrow}_{\rm rad}$ and $\overline{P}^{\downarrow}_{\rm rad}$, it is remarkable that in figure 4 the layer contributions to the total ohmic energy loss, $\overline{P}_{{\rm ohm},l}(\overline{\omega})$, show large differences at frequencies $\overline{\omega} < 13.3$ and $\overline{\omega} < 4.2$ in the panels (a) and (b), respectively. We suggest that, in the case of a TLG with the interlayer separation $\overline{d} = 0.1$, differences seen in figure 4(a) at $\overline{\omega} \lesssim 3$ may be related to different distributions of the weights for the three HDPP modes in the joint distributions $\overline{F}_{{\rm ohm},l}(\overline{k}, \overline{\omega})$ for each graphene layer, as implied by different widths of those modes in the panels (a)–(c) of the figure 2. Namely, the largest difference among those distributions is that $\overline{F}_{{\rm ohm},2}(\overline{k}, \overline{\omega})$ for the middle graphene layer is missing a contribution from the HDPP mode with the middle dispersion $\overline{\omega}_2$, whereas that mode makes the largest contribution to the ohmic losses in the bottom and the top graphene layers. Accordingly, one sees in figure 4(a) that the integrated ohmic losses in the outer layers, $\overline{P}_{{\rm ohm},1}(\overline{\omega})$ and $\overline{P}_{{\rm ohm},3}(\overline{\omega})$, have similar values for $0.5 \lesssim \overline{\omega} \lesssim 3$, which exceed the value of the integrated ohmic loss in the middle layer, $\overline{P}_{{\rm ohm},2}(\overline{\omega})$. On the other hand, at frequencies $\overline{\omega} < 0.1$, one observes that $\overline{P}_{{\rm ohm},2}(\overline{\omega})$ and $\overline{P}_{{\rm ohm},3}(\overline{\omega})$ take similar values for the middle and top graphene layers, which are mostly determined by the resonant contributions of the HDPP with the lowest lying dispersion, $\overline{\omega}_1$. Those values are seen to be smaller than the value of $\overline{P}_{{\rm ohm},1}(\overline{\omega})$ at frequencies $\overline{\omega} < 0.1$, which may be tentatively ascribed to increased contribution to the ohmic energy loss at frequencies lower than $\overline{\omega}_1$ due to the strongly asymmetric Fano resonance near $\overline{\omega} = \overline{\omega}_1(\overline{k})$ for the bottom layer, as displayed in the inset to figure 2(c).

In the panel (a) of figure 4, one notices that the integrated ohmic energy losses $\overline{P}_{{\rm ohm},l}(\overline{\omega})$ exhibit peculiar and rather different structures in the frequency range $3 \lesssim \overline{\omega} \lesssim 13$. It is interesting that a superposition of those structures gives rise to a well defined and broad peak at $\overline{\omega} \approx 8$ in the total integrated ohmic energy loss distribution $\overline{P}_{\rm ohm}(\overline{\omega})$. When the interlayer separation is increased to $\overline{d} = 1$ in the panel (b), those structures become even more complex and they move to a lower frequency range of $0.5 \lesssim \overline{\omega} \lesssim 5$. In that case, the total integrated ohmic energy loss distribution exhibits two peaks at $\overline{\omega} \approx 1$ and $\overline{\omega} \approx 3$. This behavior of the layer decomposition and the total ohmic energy loss distributions for the TLG is surprisingly similar to the behavior of those distributions for a DLG with the same interlayer separations, discussed in figure 5 of [14]. We shall demonstrate below that this similarity is not coincidental, but is rather universal for MLG with $N > 2$ in a regime of intermediate optical thickness. Namely, we argue that the DPP hybridization in such MLG is governed mostly by the electromagnetic interaction between the *nearest-neighbor* graphene layers, which should be similar to the hybridization taking place in a DLG. This assertion is further tested in the SM. In that respect, it is worthwhile mentioning that an analysis of the modal decomposition of the total energy losses in a DLG showed that single- and double-peak structures in $\overline{P}_{\rm ohm}(\overline{\omega})$ result from an onset of interference in the excitation of the two HDPP modes at frequencies $\overline{\omega} \sim \pi\beta/\overline{d}$ (see figure 6 in [14]). We suggest that a similar mechanism may be responsible for the single- and double–peak structures observed in $\overline{P}_{\rm ohm}(\overline{\omega})$ for the TLG in the panels (a) and (b) of figure 4.

From the features seen in the distributions in figures 3 and 4, one may conclude that large qualitative differences may arise when the interlayer distance increases from a sufficiently small value for which the MLG may be considered as optically thin, at least in a range of small frequencies, to a large value, $\overline{d} \sim 1$, for which the retardation effects should be strong. Therefore, we next explore the effect of increasing the number of graphene layers and analyze changes in the integrated energy loss spectra as we decrease the interlayer distance further into the regime of optically thin MLG. So, in figure 5 we show the total ohmic loss, $\overline{P}^{(N)}_{\rm ohm}(\overline{\omega})$, and the total radiation loss, $\overline{P}^{(N)}_{\rm rad}(\overline{\omega})$, for $N = 1$, 2, 3, 4 and 5 graphene layers and for $\overline{d} = 0.001$, 0.01, 0.1 and 1. Also shown (by dotted lines) are the results for the integrated ohmic energy loss in an SLG, $\overline{P}^{\rm SLG}_{\rm ohm}[\overline{\sigma}_N(\overline{\omega}), \overline{\omega}]$, where the effective conductivity is given by $\overline{\sigma}_N(\overline{\omega}) = N\overline{\sigma}(\overline{\omega})$, with $\overline{\sigma}(\overline{\omega})$ given by the Drude model in equation (14). Those results are expected to provide a good approximation for $\overline{P}^{(N)}_{\rm ohm}(\overline{\omega})$ in an optically thin N-layer graphene structure [18, 22, 24].

In order to quantify the criterion for an optically thin MLG regarding the ohmic loss, we note that the approximation $\sigma_N \approx N\sigma$ follows from equation (1) when all the exponential factors can be replaced by unity, i.e., when $(N-1)\overline{q}\overline{d} \ll 1$. In order to estimate relevant values of the factor $\overline{q} = \sqrt{\overline{k}^2 - \overline{\omega}^2}$, we may temporarily neglect the role of damping and use the approximate expressions for the HDPP dispersion relations obtained from the approximation $\sigma_N \approx N\sigma$ itself. Thus, for the highest lying mode, using $\overline{\omega} \approx \overline{\omega}^{\rm appr}_N(\overline{k})$ gives a criterion for an optically thin MLG in the form $\overline{\omega} \ll \sqrt{2/\overline{d}}$, independent of N. A rough estimate of the same criterion for lower-lying, quasi-acoustic dispersion relations may be obtained, at least for sufficiently thin MLG, such that $\overline{d} \ll 1$. With that assumption, an expansion of the exponential factors in equation (1) to the leading order in $\overline{d}$ gives $\overline{\omega}_j \sim \phi_j\sqrt{\overline{d}}\ \overline{k}$ in the limit of long wavelengths, where ϕ_j is a numerical factor of order one for all $j = 1, 2, \ldots N-1$. Thus, replacing $\overline{k} \sim \overline{\omega}/\sqrt{\overline{d}}$ in $(N-1)\overline{q}\overline{d} \ll 1$ gives a criterion for optically thin MLG in the form $\overline{\omega} \ll 1/(N\sqrt{\overline{d}})$. Accordingly, one

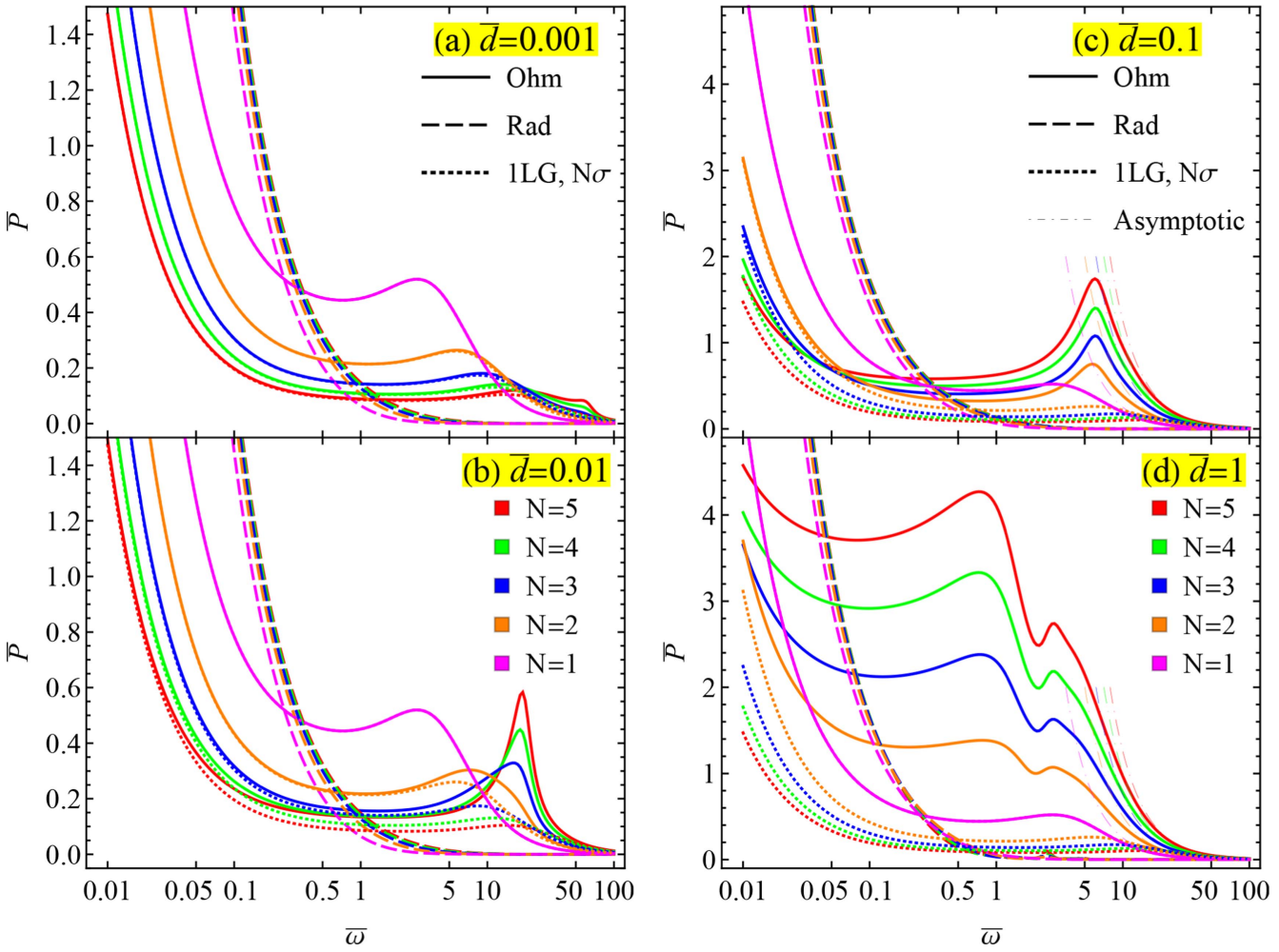

Figure 5. The total integrated ohmic energy loss, $\overline{P}^{(N)}_{\rm ohm}(\overline{\omega})$ (solid lines), and the total radiation loss, $\overline{P}^{(N)}_{\rm rad}(\overline{\omega})$ (dashed lines), both normalized with $P_c = \frac{4}{\pi}\frac{1}{\varepsilon_F}$, are shown for multi-layer structures with $N = 1$, 2, 3, 4 and 5 graphene layers, having several interlayer distances: (a) $\overline{d} = 0.001$, (b) 0.01, (c) 0.1 and (d) 1. Also shown (by dotted lines) is the integrated ohmic energy loss in a single-layer graphene, $\overline{P}^{\rm SLG}_{\rm ohm}[\overline{\sigma}_N, \overline{\omega}]$, evaluated with an effective conductivity $\overline{\sigma}_N = N\overline{\sigma}$ for $N = 1$, 2, 3, 4 and 5 with $\overline{\sigma}$ given in equation (14). The thin dashed–dotted lines show the high-frequency asymptotics of the total integrated ohmic energy loss, $\overline{P}^{(N)}_{\rm ohm}(\overline{\omega}) \sim 2\pi N/(\beta\overline{\omega})^2$, with $\beta = v/c = 0.5$.

notices in figure 5(a) that the distribution $\overline{P}^{\rm SLG}_{\rm ohm}[N\overline{\sigma}(\overline{\omega}), \overline{\omega}]$ provides a very good approximation to $\overline{P}^{(N)}_{\rm ohm}(\overline{\omega})$ at frequencies $\overline{\omega} \lesssim 10$ for all N values. This seems to be consistent with the criterion $\overline{\omega} \ll \sqrt{2/\overline{d}}$, showing that the HDPP mode with the highest-lying eigenfrequency likely dominates in the case of the thinnest MLG with $\overline{d} = 0.001$ studied in figure 5(a). We remark that the corresponding physical distance of $d = 48$ nm is commensurate with the interlayer distances used in experiments [18, 22]. However, a gradual deterioration of the approximation $\overline{P}^{(N)}_{\rm ohm}(\overline{\omega}) \approx \overline{P}^{\rm SLG}_{\rm ohm}[N\overline{\sigma}(\overline{\omega}), \overline{\omega}]$ is observed in the panels (b) and (c) of figure 5 for frequencies above some critical value, which decreases when both $\overline{d}$ and N increase. This seems to be consistent with the criterion $\overline{\omega} \ll 1/(N\sqrt{\overline{d}})$, indicating an increasing role of the $N-1$ quasi-acoustic HDPP modes with increasing inter-layer distance, which start affecting the ohmic energy loss at shorter wavelengths and hence higher frequencies.

A close inspection of the low-frequency dependence of the $\overline{P}^{(N)}_{\rm ohm}(\overline{\omega})$ distributions in figures 5(a) and (b) shows that the integrated ohmic energy loss decreases in an inverse proportion to N for frequencies $\overline{\omega} \lesssim \overline{\gamma} = 0.05$ for optically thin MLG. The reason for this behavior is not immediately obvious, but it may be conjectured by recalling that the ohmic energy loss at low frequencies is dominated by dissipative processes in graphene [13, 14]. Namely, the dc resistivity of a SLG may be represented, in reduced units, as $\overline{\rho} = 1/\overline{\sigma}(0) = \pi\overline{\gamma}$, so that the dissipative processes in an optically thin MLG with N graphene layers may be represented by a *parallel* connection of N resistors with the effective resistivity given by $\overline{\rho}_N \approx \overline{\rho}/N = \pi\overline{\gamma}/N$. This argument may be made more quantitative by considering the analytical result for $\overline{P}^{\rm SLG}_{\rm ohm}[N\overline{\sigma}(\overline{\omega}), \overline{\omega}]$ for SLG obtained in [13], which we have used in this work to calculate the dotted curves in figure 5 with $\overline{\sigma}(\overline{\omega})$ given by the Drude model with finite damping rate $\overline{\gamma}$ in equation (14). Since $\overline{P}^{(N)}_{\rm ohm}(\overline{\omega}) \approx \overline{P}^{\rm SLG}_{\rm ohm}[N\overline{\sigma}(\overline{\omega}), \overline{\omega}]$ to a very good approximation at low frequencies in figures 5(a) and (b), an analysis of the $\overline{\omega} \to 0$ behavior of $\overline{P}^{\rm SLG}_{\rm ohm}[N\overline{\sigma}(\overline{\omega}), \overline{\omega}]$

shows that

$$\overline{P}_{\rm ohm}^{(N)}(\overline{\omega}) \sim \frac{\beta^2}{4N}\frac{\overline{\gamma}}{\overline{\omega}}\left[4\ln\left(\frac{2N}{\beta\overline{\gamma}}\right) + \beta^{-2} - 4 - \ln\left(\beta^{-2} - 1\right)\right], \tag{15}$$

to the leading order in $\overline{\gamma}$. This result exposes the predominantly $1/N$ dependence of the integrated ohmic energy loss at frequencies $\overline{\omega} \lesssim \overline{\gamma} = 0.05$ for optically thin MLG.

Turning our attention to the regime of higher frequencies and larger $\overline{d}$ values, we recall from figure 4 that interferences among the HDPP modes give rise to the peak structures in the ohmic energy loss spectra for $N = 3$ with $\overline{d} = 0.1$ and 1 in a regime that may be considered as intermediate between optically thin and optically thick TLGs. Considering the MLG in figure 5, peak structures are barely visible at high frequencies for $\overline{d} = 0.001$ in the panel (a), whereas they seem to gradually increase in magnitude with increasing $\overline{d}$ and N values, as seen in the panels (b)–(d) of that figure. Specifically, single-peak structures appear for $N \geqslant 2$ in the range $10 \lesssim \overline{\omega} \lesssim 20$ for $\overline{d} = 0.01$ in the panel (b) and at $\overline{\omega} \approx 8$ for $\overline{d} = 0.1$ in the panel (c), whereas a double peak structure appears at $\overline{\omega} \approx 1$ and $\overline{\omega} \approx 3$ for $\overline{d} = 1$ in the panel (d). While the peak position in the panel (b) increases in the interval $10 \lesssim \overline{\omega} \lesssim 20$ with increasing N values, it is remarkable that the peak structures in the panels (c) and (d) exhibit both the shape *and* position, which are rather independent from the number of layers for $N \geqslant 2$. This may be qualitatively explained by an argument that, for thicker MLG with $\overline{d} = 0.1$ and $\overline{d} = 1$, the interferences giving rise to the peak structures are mainly governed by the distance between *neighboring* graphene layers, so that the effect of increasing N is merely to increase the magnitude of the peaks. More specifically, it seems that the peaks in the panels (c) and (d) for $N > 2$ are replicas of the peak structure of a DLG, with their magnitudes that scale with the number of layers N. (These notions are further tested in the SM by using a nearest-neighbor approximation in solving equation (1) to generate the curves in figure S2.)

Such scaling of the total ohmic energy loss with N at high frequencies may be deduced by considering the limit of an optically thick MLG consisting of N *independent* graphene layers, which formally arises when the exponential factors in equation (1) may be set to zero, i.e., when $\overline{q}\overline{d} \gg 1$ for sufficiently short wavelengths. Given that in this limit the dispersion relations of all N HDPP modes in an MLG approach the dispersion of a SLG, as shown in figure S1 of the SM, one may use the non-retarded form of the SLG dispersion, $\overline{\omega} = \sqrt{2\overline{k}}$, to obtain a criterion for an optically thick MLG as $\overline{\omega} \gg \sqrt{2/\overline{d}}$. Because in that regime we may write $\overline{P}_{{\rm ohm},l}^{(N)}(\overline{\omega}) \approx \overline{P}_{\rm ohm}^{\rm SLG}[\overline{\sigma}(\overline{\omega}), \overline{\omega}]$ for each graphene layer with the conductivity $\overline{\sigma}(\overline{\omega})$ given in equation (14), the total integrated ohmic energy loss in an MLG becomes $\overline{P}_{\rm ohm}^{(N)}(\overline{\omega}) \approx N\overline{P}_{\rm ohm}^{\rm SLG}[\overline{\sigma}(\overline{\omega}), \overline{\omega}]$ for $\overline{\omega} \gg \sqrt{2/\overline{d}}$. Using the analytical result for $\overline{P}_{\rm ohm}^{\rm SLG}[\overline{\sigma}(\overline{\omega}), \overline{\omega}]$ obtained in [13] for SLG in the limit of zero damping, we can easily deduce that the asymptotic behavior of the total ohmic energy loss in an optically thick MLG with $N > 1$ at large frequencies has the form given by $\overline{P}_{\rm ohm}^{(N)}(\overline{\omega}) \sim 2\pi N/(\beta\overline{\omega})^2$, which is indicated by the thin dashed–dotted curves in figures 5(c) and (d).

Finally, it is remarkable to observe in figure 5 that the total integrated radiation energy loss $\overline{P}_{\rm rad}^{(N)}(\overline{\omega})$ in an MLG with N layers is largely independent of the interlayer distance and is only weakly increasing with increasing N at sub-THz frequencies. As in figure 4, this may be explained by the fact that only the charge carrier oscillations in the outer layers give rise to the radiation emitted in the far field region, whereas the energy flux due to radiating fields experiences destructive interference in the regions between graphene layers within an MLG.

4. Conclusion

We have studied the ohmic and radiation energy losses in an MLG with N layers traversed by a fast charged particle under normal incidence. Assuming equal interlayer distances d and equal doping densities n of the constituent graphene layers, we have explored the limits of both optically thin MLG and optically thick MLG in terms of plasmon hybridization among the constituent graphene layers in the THz range of frequency ω. By adopting the Drude model for the optical conductivity of each graphene layer, $\sigma(\omega)$, we found that an optically thin/thick MLG is roughly defined by values of the ohmic energy loss $\hbar\omega$ being much smaller/larger than the parameter $\sim e\sqrt{\varepsilon_F/d}$, where ε_F is the Fermi energy in individual graphene layers.

Performing a layer-wise decomposition of the ohmic energy loss in a TLG ($N = 3$), we have found that the hybridized plasmon mode with the middle eigenfrequency is not excited in the middle graphene layer, which was explained by a double degeneracy of the corresponding charge oscillation patterns in that layer. This observation may be of technological interest, as the excitation of such mode in the middle layer appears to be efficiently prevented by the presence of the outer graphene layers in a TLG, thereby providing a protected plasmonic channel.

On the other hand, we have observed important differences between the distributions of the ohmic energy losses in the outer graphene layers in a TLG, as well as between the angular distributions of the transition radiation emitted in the half-spaces on either side of the TLG. Such differences indicate asymmetry of those processes with respect to the order in which graphene layers are traversed by the external charged particle, pointing to the retardation effects as the likely cause of the asymmetry. As a possible manifestation of those effects in a TLG, we have found that the ohmic energy loss distribution in the graphene layer, which is first traversed by the external charged particle, exhibits a Fano resonance near the lowest-lying hybridized plasmon eigenfrequency, whereas such resonance is not observed in the graphene layer that is traversed last.

Whereas the observed asymmetry in the angular distributions of the transition radiation should be detectable by using parabolic mirrors in a TEM setting, we have found that

the integrated distribution of the radiative energy loss is rather independent of both the interlayer distance and the number of graphene layers in an MLG. This is explained by the fact that only charge carrier oscillations in the outer layers in an MLG give rise to the radiation emitted in the far field region, whereas the energy flux due to radiating fields experiences cancellation due to destructive interference in the interior regions of the MLG.

We have further observed that prominent peak structures develop in the integrated ohmic energy loss distributions at the supra-THz frequencies due to interferences between hybridized plasmon modes in MLG systems with $N \geqslant 2$. Those peaks were found to be very similar in shape and position to the peak structures in a DLG ($N = 2$), but with their magnitudes that scale with the number of graphene layers for $N > 2$. This is explained by asserting that, in an MLG that is intermediate between the optically thin and optically thick systems, plasmon hybridization is governed mostly by the electromagnetic interaction between the nearest-neighbor graphene layers.

For an optically thin MLG with N layers, we have confirmed that representing its structure as a single layer with the effective conductivity $N\sigma$ provides a very good approximation to the distribution of the integrated ohmic energy loss at low frequencies. Moreover, the magnitude of that distribution was found to decrease in an inverse proportion to N at low frequencies, which was explained by recalling that graphene's response at such frequencies is dominated by dissipative processes. Given that the plasmon damping is generally unwanted process in graphene-based nano-photonic and nano-plasmonic devices, whereas the damping rate is largely unknown parameter in modeling of such devices, it is therefore remarkable that the effects of damping may be efficiently suppressed, at least at sub-THz frequencies, by using optically thin MLG with increasing number of graphene layers [40, 41].

We remark that the above conclusions are deduced for a system represented by a stack of graphene layers suspended in free space. In most experimental setups, there is a substrate, which would probably affect the observed asymmetry with respect to the traversal order of graphene layers by the incident charged particle. Moreover, a possible presence of dielectric spacers between graphene layers would affect the hybridization between their plasmon modes, not only via screening provided by their dielectric constant(s), but also by additional hybridization of graphene plasmons with phonon modes in those layers [40]. On the other hand, the presence of a substrate and dielectric spacers would also strongly affect the radiation spectra due to Cherenkov radiation in those materials at sufficiently large particle speeds, as well as transition radiation arising when this particle traverses a boundary between materials with different dielectric constants.

Acknowledgments

Argentinean team acknowledges the financial support from CONICET (PIP 11220120100374) from Argentina. ZLM acknowledges support from the Natural Sciences and Engineering Research Council of Canada (grant No. 2016-03689).

ORCID iDs

Zoran L Mišković https://orcid.org/0000-0003-3882-8930

References

[1] Rana F 2008 *IEEE Trans. Nanotechnol.* **7** 91–9
[2] Low T and Avouris P 2014 *ACS Nano* **8** 1086–101
[3] Garcia de Abajo F J 2014 *ACS Photon.* **1** 135–52
[4] Das Sarma S, Adam S, Hwang E H and Rossi E 2011 *Rev. Mod. Phys.* **83** 407–70
[5] Koppens F H L, Chang D E and Garcia de Abajo F J 2011 *Nano Lett.* **11** 3370–7
[6] Xiao S, Zhu X, Li B H and Mortensen N A 2016 *Front. Phys.* **11** 117801
[7] Eberlein T, Bangert U, Nair R R, Jones R, Gass M, Bleloch A L, Novoselov K S, Geim A and Briddon P R 2008 *Phys. Rev.* B **77** 233406
[8] Nelson F J, Idrobo J C, Fite J D, Miskovic Z L, Pennycook S J, Pantelides S T, Lee J U and Diebold A C 2014 *Nano Lett.* **14** 3827–31
[9] Politano A and Chiarello G 2014 *Nanoscale* **6** 10927–40
[10] Zhan T, Han D, Hu X, Liu X, Chui S T and Zi J 2014 *Phys. Rev.* B **89** 245434
[11] Liu S, Zhang C, Hu M, Chen X, Zhang P, Gong S, Zhao T and Zhong R 2014 *Appl. Phys. Lett.* **104** 201104
[12] Zhang K C, Chen X X, Sheng C J, Ooi K J A, Ang L K and Yuan X S 2017 *Opt. Express* **25** 20477–85
[13] Miskovic Z L, Segui S, Gervasoni J L and Arista N R 2016 *Phys. Rev.* B **94** 125414
[14] Akbari K, Miskovic Z L, Segui S, Gervasoni J L and Arista N R 2017 *ACS Photon.* **4** 1980–92
[15] Garcia de Abajo F J 2010 *Rev. Mod. Phys.* **82** 209–75
[16] Coenen T, Brenny B J, Vesseur E J and Polman A 2015 *MRS Bull.* **40** 359–65
[17] Stoger-Pollach M, Kachtik L, Miesenberger B and Retzl P 2017 *Ultramicroscopy* **173** 31–5
[18] Yan H, Li X, Chandra B, Tulevski G, Wu Y, Freitag M, Zhu W, Avouris P and Xia F 2012 *Nat. Nanotechnol.* **7** 330–4
[19] Liu M, Yin X and Zhang X 2012 *Nano Lett.* **12** 1482–5
[20] Tredicucci A and Vitiello M S 2014 *IEEE J. Sel. Top. Quantum Electron.* **20** 130–8
[21] Francescato Y, Giannini V, Yang J, Huang M and Maier S A 2014 *ACS Photon.* **1** 437–43
[22] Gomez-Diaz J S, Moldovan C, Capdevila S, Romeu J, Bernard L S, Magrez A, Ionescu A M and Perruisseau-Carrier J 2015 *Nat. Commun.* **6** 6334
[23] Rodrigo D, Tittl A, Limaj O, Garcia de Abajo F J, Pruneri V and Altug H 2017 *Light Sci. Appl.* **6** e16277
[24] Menabde S G, Mason D R, Kornev E E, Lee C and Park N 2016 *Sci. Rep.* **6** 21523
[25] Mencarelli D, Pierantoni L, Stocchi M and Bellucci S 2016 *Appl. Phys. Lett.* **109** 093103
[26] Ruan B, Guo J, Wu L, Zhu J, You Q, Dai X and Xiang Y 2017 *Sensors* **17** 1924
[27] Huang Y, Zhong S, Yao H and Cui D 2017 *IEEE Photon. J.* **9** 1–10
[28] Hwang E H and Das Sarma S 2009 *Phys. Rev.* B **80** 205405
[29] Badalyan S M and Peeters F M 2012 *Phys. Rev.* B **85** 195444
[30] Gomez-Santos G and Stauber T 2012 *Europhys. Lett.* **99** 27006

[31] Profumo R E V, Asgari R, Polini M and MacDonald A H 2012 *Phys. Rev.* B **85** 085443
[32] Zhu J J, Badalyan S M and Peeters F M 2013 *Phys. Rev.* B **87** 085401
[33] Stauber T 2014 *J. Phys.: Condens. Matter* **26** 123201
[34] Stauber T and Gomez-Santos G 2012 *Phys. Rev.* B **85** 075410
[35] Alonso-Gonzalez P *et al* 2016 *Nat. Nanotechnol.* **12** 31–5
[36] Gumbs G, Iurov A, Wu J Y, Lin M F and Fekete P 2016 *Sci. Rep.* **6** 21063
[37] Sen G, Min H, Renbing Z, Xiaoxing C, Tao Z and Shenggang L 2015 *Terahertz Sci. Technol.* **8** 170–8
[38] Batrakov K and Maksimenko S 2017 *Phys. Rev.* B **95** 205408
[39] Novko D, Sunjic M and Despoja V 2016 *Phys. Rev.* B **93** 125413
[40] Despoja V, Djordjevic T, Karbunar L, Radovic I and Miskovic Z L 2017 *Phys. Rev.* B **96** 075433
[41] Zhao T, Hu M, Zhong R, Gong S, Zhang C and Liu S 2017 *Appl. Phys. Lett.* **110** 231102
[42] Jackson J D 1999 *Classical Electrodynamics* 3rd edn (New York: Wiley)
[43] Lundeberg M B *et al* 2017 *Science* **357** 187–91
[44] Lukyanchuk B, Zheludev N I, Maier S A, Halas N J, Nordlander P, Giessen H and Chong C T 2010 *Nat. Mater.* **9** 707–15